Available online at www.sciencedirect.com
SCIENCE DIRECT
Thermochimica Acta 443 (2006) 98–104
thermochimica acta
www.elsevier.com/locate/tca

Thermodynamics of $BaNd_2Fe_2O_7$(s) and $BaNdFeO_4$(s) in the system Ba–Nd–Fe–O

S.K. Rakshit *, S.C. Parida, S. Dash, Ziley Singh, V. Venugopal

Product Development Section, Radiochemistry & Isotope Group, Bhabha Atomic Research Centre, Mumbai 400085, India

Received 16 June 2005; received in revised form 20 December 2005; accepted 27 December 2005
Available online 20 February 2006

Abstract

Two compounds, $BaNd_2Fe_2O_7$(s) and $BaNdFeO_4$(s) in the quaternary system Ba–Nd–Fe–O were prepared by citrate–nitrate gel combustion route and characterized by X-ray diffraction analysis. Heat capacities of these two oxides were measured in two different temperature ranges: (i) 130–325 K and (ii) 310–845 K, using a heat flux type differential scanning calorimeter. Two different types of solid-state electrochemical cells with CaF_2(s) as the solid electrolyte were employed to measure the e.m.f. as a function of temperature. The standard molar Gibbs energies of formation of these quaternary oxides were calculated as a function of temperature from the e.m.f. data. The standard molar enthalpies of formation from elements at 298.15 K, $\Delta_f H^\circ_m$ (298.15 K) and the standard entropies, S°_m (298.15 K) of these oxides were calculated by the second law method. The values of $\Delta_f H^\circ_m$ (298.15 K) and S°_m (298.15 K) obtained for $BaNd_2Fe_2O_7$(s) are: $-2756.9\,kJ\,mol^{-1}$ and $234.0\,J\,K^{-1}\,mol^{-1}$ whereas those for $BaNdFeO_4$(s) are: $-2061.5\,kJ\,mol^{-1}$ and $91.6\,J\,K^{-1}\,mol^{-1}$, respectively.

Keywords: Quaternary oxides; Thermodynamic properties; Heat capacity; Solid-state electrochemical cell; Differential scanning calorimetry

1. Introduction

The quaternary oxides in the system M–RE–Fe–O (M = Ca, Sr, Ba, RE = rare earths, La, Ce, . . ., Lu) have been the subject of great interest owing to their interesting magnetic properties [1]. Some of the complex oxides in these systems are promising candidates as host materials for containment of radioactive wastes [2]. As a part of systematic studies on the quaternary oxides in the series M–RE–Fe–O, thermodynamic studies on the system Ba–Nd–Fe–O has been carried out. The two most important stoichiometric compounds are $BaNd_2Fe_2O_7$(s) and $BaNdFeO_4$(s), the latter compound having two-dimensional magnetic properties. These two compounds lie on the line joining the two boundary compounds $NdFeO_3$(s) and BaO(s) of the pseudo-ternary system Nd_2O_3–Fe_2O_3–BaO. Hence, one can obtain these quaternary compounds by successive addition of BaO to $NdFeO_3$ which at first leads to the formation of $BaNd_2Fe_2O_7$(s) and then $BaNdFeO_4$(s). Formation of these quaternary oxides by successive addition of BaO to $NdFeO_3$, helps in conceptualizing the solid-state galvanic cell based on CaF_2(s) solid electrolyte for the e.m.f. measurements. In the present study, the standard molar heat capacities and the standard molar Gibbs energies of formation ($\Delta_f G^\circ_m$) of these quaternary compounds have been determined by differential scanning calorimetry and solid-state electrochemical cells employing CaF_2(s) as fluoride ion conducting solid electrolyte.

2. Experimental

2.1. Materials preparation

Stoichiometric proportions of preheated Nd_2O_3(s) (LEICO Industries Inc., mass fraction 0.9985), $Ba(NO_3)_2$ (E. Merck, India, mass fraction 0.998) and $Fe(NO_3)_3{\cdot}9H_2O$(s) (Qualigens Fine Chemicals, mass fraction 0.99) were dissolved in dilute HNO_3. Excess amount of citric acid (E. Merck, mass fraction 0.995) was added to the solution to assist in complete dissolution. The solution was heated on a hot plate at $T = 375$ K to remove water and oxides of nitrogen. A gel was formed which was heated at 450 K to dryness. The residue was ground in an agate mortar and heated at $T = 1473$ K in air for 72 h with

* Corresponding author. Tel.: +91 22 25590648; fax: +91 22 25505345.
E-mail addresses: swarup_kr@rediffmail.com, swarupkr@magnum.barc.ernet.in (S.K. Rakshit).

0040-6031/$ – see front matter © 2006 Elsevier B.V. All rights reserved.
doi:10.1016/j.tca.2005.12.020

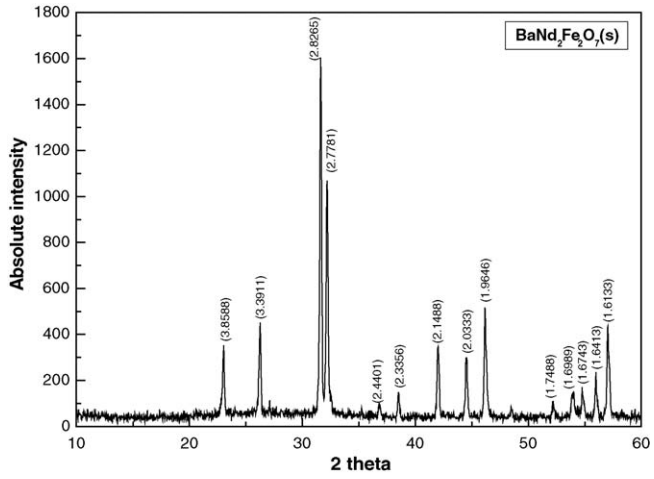

Fig. 1. XRD pattern of $BaNd_2Fe_2O_7$(s). Parameters shown within brackets '( )' represent *d*-values.

two intermediate grindings. The products were identified as $BaNd_2Fe_2O_7$(s) and $BaNdFeO_4$(s) by X-ray diffraction (XRD) analysis using a DIANO X-ray diffractometer with Cu Kα radiation. The XRD patterns are shown in Figs. 1 and 2, respectively, and resemble those of $BaLa_2Fe_2O_7$(s) and $BaLaFeO_4$(s) which belong to tetragonal crystal system. Hence, the observed XRD patterns of these compounds have been indexed assuming tetragonal crystal structure using an interactive powder diffraction data interpretation and indexing program to calculate the unit cell parameters. The values are given by:

Compound	*a* (Å)	*c* (Å)	Unit cell volume (Å^3)
$BaNd_2Fe_2O_7$(s)	3.9256	20.3508	313.61
$BaNdFeO_4$(s)	3.8805	12.7873	192.55

Powder samples of $BaNd_2Fe_2O_7$(s) and $BaNdFeO_4$(s) were used for heat capacity measurements. Based on the phase relations, phase mixtures: $\{BaNd_2Fe_2O_7(s) + NdFeO_3(s) + BaF_2(s)\}$, $\{BaNdFeO_4(s) + BaNd_2Fe_2O_7(s) + BaF_2(s)\}$ and $\{CaO(s) + CaF_2(s)\}$ were mixed homogenously and pelletized using a steel die at a pressure of 100 MPa and sintered at $T = 1073$ K in purified oxygen gas for 24 h, which were subsequently used for e.m.f. measurements.

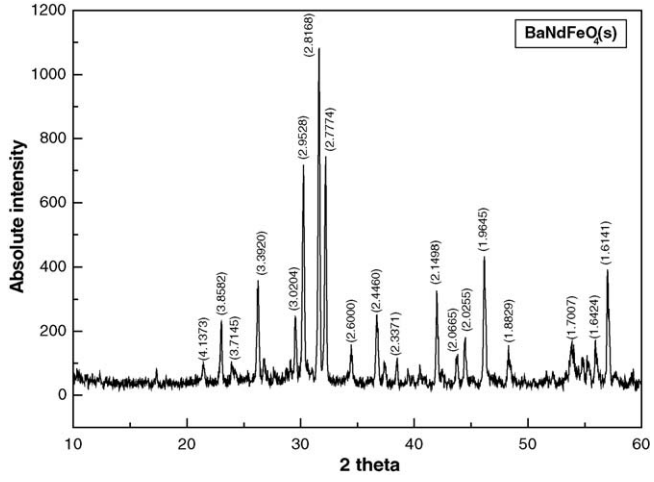

Fig. 2. XRD pattern of $BaNdFeO_4$(s). Parameters shown within brackets '( )' represent *d*-values.

2.2. Measurement of heat capacity using differential scanning calorimetry

Heat capacity measurements were carried out using a heat flux type differential scanning calorimeter, DSC 131 supplied by Setaram Instrumentation, France. Temperature calibration for the calorimeter was carried out using the phase transition temperatures of NIST reference materials (indium: $T_{fus} = 429.748$ K; tin: $T_{fus} = 505.078$ K; lead: $T_{fus} = 600.600$ K). Analar grade samples of cyclohexane ($T_{fus} = 280.1$ K, $T_{trs} = 190.0$ K), mercury ($T_{fus} = 234.316$ K), potassium nitrate ($T_{trs} = 400.850$ K) and silver sulfate ($T_{trs} = 703.150$ K) were also used to perform temperature calibration of the DSC. Heat calibration of the calorimeter was carried out using the transition heats of the above-mentioned materials.

In this heat flux DSC 131, molar heat capacity is measured by the "classical" three-step method. The precise determination of molar heat capacity at constant pressure, $C_{p,m}(T)$, requires three experiments with identical experimental conditions:

(1) The first experiment with two empty identical cells without sample to determine the zero-line for the heat flow.
(2) The second experiment with the cells and the reference sample having known $C_{p,m}(T)$.
(3) The third experiment with the cells and the sample whose heat capacity is to be determined.

The heat capacity of the sample under investigation can be calculated by a simple comparison of the heat flow rates into the sample and into the calibration substance as illustrated in literature [3]. The expression used for the calculation of heat capacity of the sample is given as:

$$C_p(T)_{sample} = \frac{HF_{sample} - HF_{blank}}{HF_{ref} - HF_{blank}} \frac{M_{ref}}{M_{sample}} C_p(T)_{ref}, \quad (1)$$

where HF_{blank}, HF_{ref} and HF_{sample} represent heat flow during first, second and third runs, respectively. $C_p(T)_{sample}$ and $C_p(T)_{ref}$ represent the heat capacities of sample and reference material, where as M_{sample} and M_{ref} represent their masses, respectively. In this method, a continuous heating mode has been used to measure the heat capacity of the substance. But, procedure of small temperature steps minimizes error in the heat capacity measurements by this method. Instead of measuring the heat flow rate curve in a single continuous step mode from initial to final temperatures, the temperature interval is divided into a number of narrow steps. With such a method, it is possible to reach the thermal equilibrium of the sample after each step of temperature. If T_i and T_{i+1} represent the initial temperature and

the next step temperature, respectively, the specific heat capacity of the step 'i' to '$(i+1)$' is calculated as follows:

$$C_p(T_i \rightarrow T_{i+1}) = \frac{\int_{T_i}^{T_{i+1}} \mathrm{HF_{sample}}\,\mathrm{d}T - \int_{T_i}^{T_{i+1}} \mathrm{HF_{blank}}\,\mathrm{d}T}{\int_{T_i}^{T_{i+1}} \mathrm{HF_{ref}}\,\mathrm{d}T - \int_{T_i}^{T_{i+1}} \mathrm{HF_{blank}}\,\mathrm{d}T} \times \frac{M_{\mathrm{ref}}}{M_{\mathrm{sample}}} C_{p_{\mathrm{ref}}} \left(\frac{T_i + T_{i+1}}{2}\right). \quad (2)$$

In the above equation, terms have their usual meanings as stated earlier. In the first experiment, two empty identical aluminum crucibles of identical masses (10^{-4} dm^3 capacity) with covering lid were kept in the sample and reference cells and the heat flow versus temperature were measured. In the second experiment, the heat flow versus temperature were measured by loading NIST synthetic sapphire (SRM-720) in the powder form (∼200 mg) into the aluminum crucible in the sample cell keeping the crucible in the reference cell empty. In the third experiment, heat flow versus temperature were measured by loading the actual experimental sample (∼200 mg) in the powder form into the aluminum crucible in the sample side and keeping the crucible in the reference side empty. Identical conditions were maintained in all the three sets of experiments.

In this study, continuous heating mode was used in the low temperature range 130–325 K and step heating mode was used in the temperature range 310–845 K. Two sets of experiments have been carried out at two different temperature ranges: (i) 130–325 K and (ii) 310–845 K to determine the molar heat capacities of $BaNd_2Fe_2O_7$(s) and $BaNdFeO_4$(s). Low temperatures below ambient was achieved using liquid nitrogen as coolant. Heat flow as a function of temperature were measured in the first temperature range from 130 to 325 K at a heating rate of 5 K min^{-1} with high purity helium as a carrier gas with a flow rate of 2 dm^3 h^{-1} and for the second temperature range 310–845 K, high purity argon was used as a carrier gas with the same flow rate and same heating rate. Heat capacity of Fe_2O_3(s) (Alfa Aesar, mass fraction 0.9999) was measured to check the accuracy of measurement and found to be within ±3.0% in lower temperature range and within ±1.5% in the high temperature range compared to the literature values [4].

2.3. Solid-state electrochemical cell with CaF_2 electrolyte

The experimental setup and the cell assembly used in this study have been explained in details by Rakshit et al. [5]. A schematic diagram of a fluoride cell used in this experiment is shown in Fig. 3. Optical grade single crystal of solid CaF_2(s) pellet of 6 mm diameter and 3 mm thickness (supplied by Solon Technologies Inc., USA) was used as fluoride ion conducting electrolyte. It is a single compartment cell with provisions for passing purified oxygen gas during the experiment and to measure the temperature of the cell near the electrode/electrolyte interface. High purity oxygen gas at 10^5 Pa was allowed to pass through successive traps of silica gels, molecular sieves, oxidized form of BTS catalyst and anhydrous magnesium perchlorate for removal of traces of H_2(g) and moisture. The reference electrode, the electrolyte and the sample electrode stacked one over the other were kept in the isothermal temperature zone of a kanthal wire wound resistance furnace. The furnace temperature was controlled within ±1 K by using a proportional temperature controller. The cell was standardized using phase mixtures of {CaO(s) + CaF_2(s)} and {MgO(s) + MgF_2(s)} as two standard electrodes. The cell can be represented as:

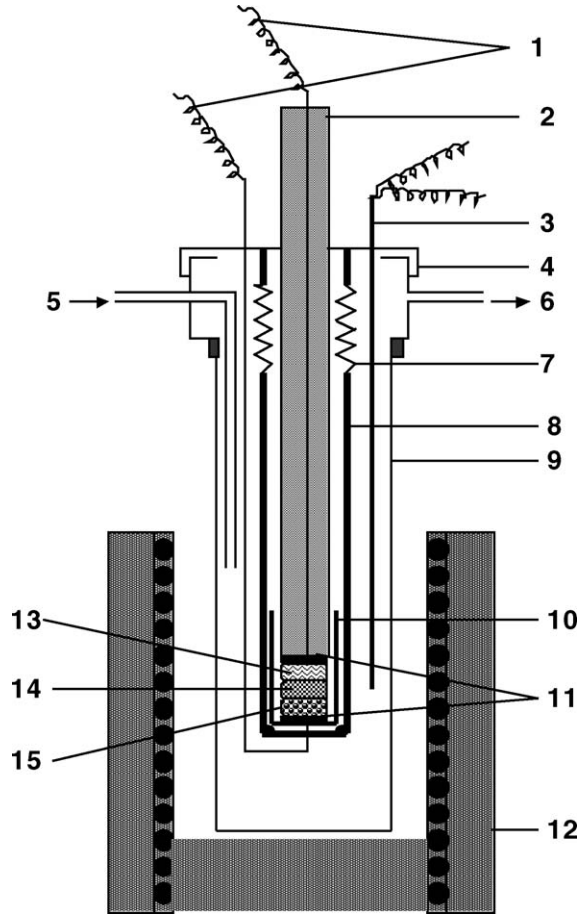

Fig. 3. Schematic diagram of the fluoride cell: (1) Pt wires, (2) alumina pressing tube, (3) thermocouple, (4) stainless steel flange, (5) gas outlet, (6) gas inlet, (7) spring, (8) quartz holder, (9) quartz tube, (10) alumina cup, (11) Pt discs, (12) kanthal wire wound furnace, (13) reference electrode, (14) CaF_2 electrolyte and (15) sample electrode.

Cell I: (−)Pt, O_2(g, 101.325 kPa)/{CaO(s) + CaF_2(s)}//CaF_2(s)//{MgO(s) + MgF_2(s)}/O_2(g, 101.325 kPa), Pt(+).

After standardization the reversible e.m.f.'s of the following solid-state galvanic cells were measured as a function of temperature:

Cell II: (−)Pt, O_2(g, 101.325 kPa)/{CaO(s) + CaF_2(s)}//CaF_2(s)//{$BaNd_2Fe_2O_7$(s) + $NdFeO_3$(s) + BaF_2(s)}/O_2(g, 101.325 kPa), Pt(+).

Cell III: (−)Pt, O_2(g, 101.325 kPa)/{$BaNdFeO_4$(s) + $BaNd_2Fe_2O_7$(s) + BaF_2(s)}//CaF_2(s)//{CaO(s) + CaF_2(s)}/O_2(g, 101.325 kPa), Pt(+).

The cell temperature close to the electrodes was measured using a pre-calibrated (ITS-90) chromel–alumel thermocouple. The cell e.m.f. (±0.02 mV) was measured by using a Keithley 614 electrometer (input impedance >10^{14} Ω). At low temperatures, stable values of e.m.f. were obtained approximately

after 72 h whereas at successive higher temperatures stability in e.m.f. values were observed within 5–6 h. The reversibility of the solid-state electrochemical cells was evaluated by micro-coulometric titration in both directions. The electrode pellets after the e.m.f. measurements were re-examined by XRD analysis and the phase compositions were found unchanged.

3. Results and discussion

3.1. Heat capacities of $BaNd_2Fe_2O_7$(s) and $BaNdFeO_4$(s)

The heat capacities of $BaNd_2Fe_2O_7$(s) and $BaNdFeO_4$(s) are determined for two different temperature ranges: (i) 130–325 K and (ii) 310–845 K and the variations of heat capacities with temperature are shown in Figs. 4 and 5, respectively. The values of heat capacities are best fitted into the following expressions in two different temperature ranges.

For the compound $BaNd_2Fe_2O_7$(s),

$$C^{\circ}_{\mathrm{p,m}}\,(\mathrm{J\,K^{-1}\,mol^{-1}})\,(\pm 3.0\%) = -30317.39 - 114.173(T\,(\mathrm{K})) + 0.25465(T\,(\mathrm{K}))^2 - 0.00025(T\,(\mathrm{K}))^3 + 8532.1981\,\ln(T\,(\mathrm{K}))$$

$$(130 \le T\,(\mathrm{K}) \le 298), \quad (3)$$

$$C^{\circ}_{\mathrm{p,m}}\,(\mathrm{J\,K^{-1}\,mol^{-1}})\,(\pm 2.5\%) = -235.4 + 0.15093(T\,(\mathrm{K})) - 1219088.9(T\,(\mathrm{K}))^{-2}$$

$$(298 \le T\,(\mathrm{K}) \le 845). \quad (4)$$

For the compound $BaNdFeO_4$(s),

$$C^{\circ}_{\mathrm{p,m}}\,(\mathrm{J\,K^{-1}\,mol^{-1}})\,(\pm 3.0\%) = -1306.34 + 29.08662(T\,(\mathrm{K})) - 0.23666(T\,(\mathrm{K}))^2 + 9.53635\times 10^{-4}(T\,(\mathrm{K}))^3 - 1.88044\times 10^{-6}(T\,(\mathrm{K}))^4 + 1.44679\times 10^{-9}(T\,(\mathrm{K}))^5 \quad (130 \le T\,(\mathrm{K}) \le 298), \quad (5)$$

$$C^{\circ}_{\mathrm{p,m}}\,(\mathrm{J\,K^{-1}\,mol^{-1}})\,(\pm 2.0\%) = 118.4 + 0.13431(T\,(\mathrm{K})) - 432731.4(T\,(\mathrm{K}))^{-2}$$

$$(298 \le T\,(\mathrm{K}) \le 845). \quad (6)$$

3.2. Standardization of solid-state galvanic cell

Prior to the e.m.f. measurements, the solid-state electrochemical cell with CaF_2(s) as an electrolyte was standardized using cell (I). The half-cell reactions at electrodes can be written as:

$$\mathrm{MgF_2(s) + 2e^- + \tfrac{1}{2}O_2(g) \rightarrow MgO(s) + 2F^-} \quad \text{(at the +ve electrode)}, \quad (7)$$

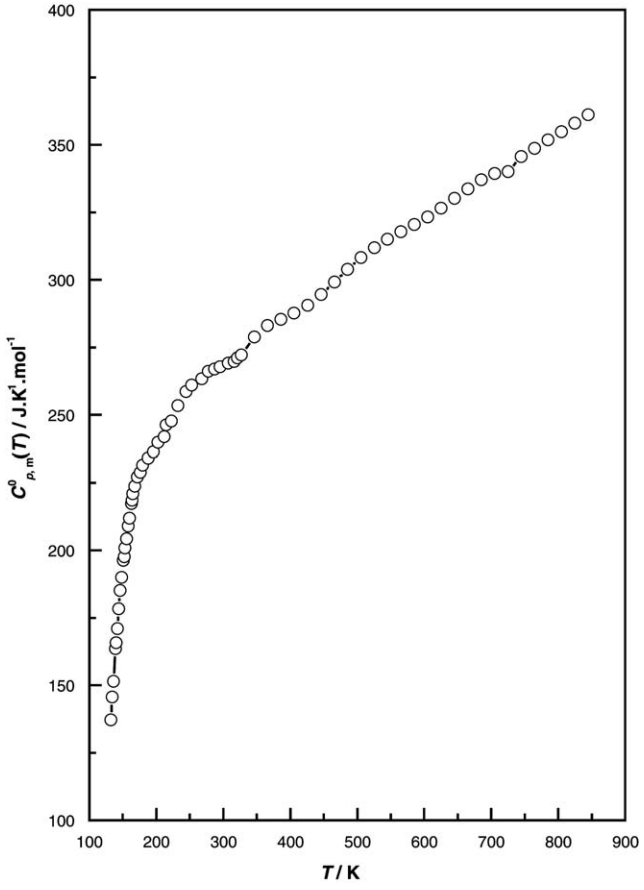

Fig. 4. Plot of molar heat capacity of $BaNd_2Fe_2O_7$(s) against temperature; (◯) experimental data.

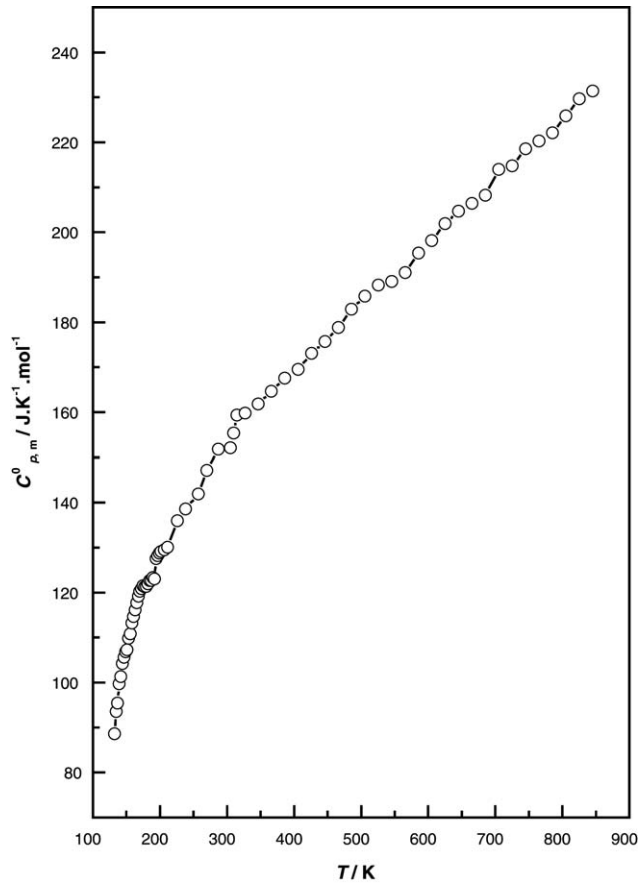

Fig. 5. Plot of molar heat capacity of $BaNdFeO_4$(s) against temperature; (◯) experimental data.

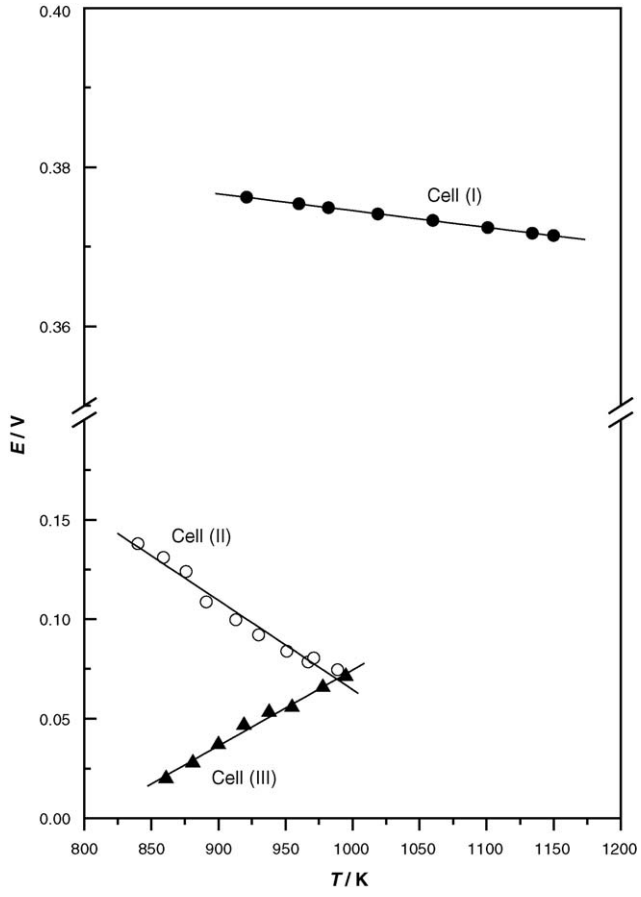

Fig. 6. Plot of e.m.f. against temperature for (●) cell (I), (◯) cell (II) and (▲) cell (III).

and

$$\mathrm{CaO(s)} + 2\mathrm{F}^- \rightarrow \mathrm{CaF_2(s)} + 2\mathrm{e}^- + \tfrac{1}{2}\mathrm{O_2(g)} \quad (\text{at the } -\text{ve electrode}). \tag{8}$$

The net virtual cell reaction can be written as:

$$\mathrm{MgF_2(s)} + \mathrm{CaO(s)} \rightarrow \mathrm{CaF_2(s)} + \mathrm{MgO(s)}. \tag{9}$$

The variation of reversible e.m.f. values obtained for cell (I) with temperature is shown in Fig. 6. The e.m.f. data were least square fitted to yield the following linear relation:

$$E_{\mathrm{I}}\,(\mathrm{V})\,(\pm 0.002) = 0.3956 - 2.1033 \times 10^{-5}(T\,(\mathrm{K})). \tag{10}$$

The Gibbs energy change for reaction (9) has been calculated from the general relation:

$$\Delta_{\mathrm{r}}G^{\circ}\,(\mathrm{J\,mol^{-1}}) = -nFE, \tag{11}$$

where n is the number of electrons involved in the half-cell reactions and F is the Faraday's constant ($F = 96486.4\,\mathrm{C\,mol^{-1}}$) and E is the e.m.f. of the cell in volts (V). The values of $\Delta_{\mathrm{r}}G^{\circ}(T)$ for reaction (9) can be calculated by using Eqs. (10) and (11) and are given by:

$$\Delta_{\mathrm{r(9)}}G^{\circ}(T)\,(\mathrm{kJ\,mol^{-1}})\,(\pm\,1.0) = -76.3 + 4.1 \times 10^{-3}(T\,(\mathrm{K})). \tag{12}$$

Table 1
Standard molar Gibbs energy of formation of auxiliary compounds taken from the literature

Compound	$\Delta_{\mathrm{f}}G^{\circ}_{\mathrm{m}}$ (kJ mol^{-1}) (800–1200 K)	Reference number
BaO(s)	$-561.4 + 0.1033(T\,(\mathrm{K}))$	[4]
BaF_2(s)	$-1191.3 + 0.1628(T\,(\mathrm{K}))$	[4]
MgO(s)	$-608.4 + 0.1151(T\,(\mathrm{K}))$	[4]
MgF_2(s)	$-1123.5 + 0.1729(T\,(\mathrm{K}))$	[4]
CaF_2(s)	$-1218.9 + 0.1618(T\,(\mathrm{K}))$	[4]
CaO(s)	$-637.4 + 0.1065(T\,(\mathrm{K}))$	[4]
$NdFeO_3$(s)	$-1345.9 + 0.2542(T\,(\mathrm{K}))$	[6]

The values of $\Delta_{\mathrm{r}}G^{\circ}(T)$ for reaction (9) obtained in this study are in good agreement (within $\pm 2.0\,\mathrm{kJ\,mol^{-1}}$) with those calculated using the values of $\Delta_{\mathrm{f}}G^{\circ}_{\mathrm{m}}(T)$ for CaF_2(s), MgF_2(s), MgO(s) and CaO(s) from literature [4] represented in Table 1.

3.3. Gibbs energy of formation for $BaNd_2Fe_2O_7$(s)

The variation of reversible e.m.f. values of cell (II) as a function of temperature is shown in Fig. 6. The e.m.f. data were least squares fitted to yield the following linear relation:

$$E_{\mathrm{II}}\,(\mathrm{V})\,(\pm 0.004) = 0.5124 - 4.4785 \times 10^{-4}(T\,(\mathrm{K})) \quad (840 \le T\,(\mathrm{K}) \le 989). \tag{13}$$

The half-cell reactions associated with cell (II) can be written as:

$$\mathrm{BaF_2(s)} + 2\mathrm{NdFeO_3(s)} + \tfrac{1}{2}\mathrm{O_2(g)} + 2\mathrm{e}^- \rightarrow \mathrm{BaNd_2Fe_2O_7(s)} + 2\mathrm{F}^- \quad (\text{at } +\text{ve electrode}), \tag{14}$$

and

$$\mathrm{CaO(s)} + 2\mathrm{F}^- \rightarrow \mathrm{CaF_2(s)} + \tfrac{1}{2}\mathrm{O_2(g)} + 2\mathrm{e}^- \quad (\text{at } -\text{ve electrode}). \tag{15}$$

The net virtual cell reaction associated with cell (II) can be written as:

$$\mathrm{CaO(s)} + 2\mathrm{NdFeO_3(s)} + \mathrm{BaF_2(s)} \rightarrow \mathrm{BaNd_2Fe_2O_7(s)} + \mathrm{CaF_2(s)}. \tag{16}$$

The Gibbs energy change, $\Delta_{\mathrm{r}}G^{\circ}(T)$, for reaction (16) can be calculated by using Eqs. (11) and (13) and can be given by:

$$\Delta_{\mathrm{r(16)}}G^{\circ}(T)\,(\mathrm{kJ\,mol^{-1}})\,(\pm 0.7) = -98.89 + 0.0864(T\,(\mathrm{K})) \quad (840 \le T\,(\mathrm{K}) \le 989). \tag{17}$$

The standard molar Gibbs energy of formation, $\Delta_{\mathrm{f}}G^{\circ}_{\mathrm{m}}$ ($BaNd_2Fe_2O_7$, s) was obtained by using Eq. (17) and the values of $\Delta_{\mathrm{f}}G^{\circ}_{\mathrm{m}}(T)$ for CaF_2(s), BaF_2(s) and CaO(s) from Table 1 and $\Delta_{\mathrm{f}}G^{\circ}_{\mathrm{m}}(T)$ for $NdFeO_3$(s) from Parida et al. [6]. The values are given by:

$$\Delta_{\mathrm{f}}G^{\circ}_{\mathrm{m}}\,(\mathrm{BaNd_2Fe_2O_7,\,s})\,(\mathrm{kJ\,mol^{-1}})\,(\pm 2.9) = -3400.5 + 0.6987(T\,(\mathrm{K})) \quad (840 \le T\,(\mathrm{K}) \le 989). \tag{18}$$

Table 2
Thermodynamic functions for $BaNd_2Fe_2O_7$(s) and $BaNdFeO_4$(s)

Compound	$\Delta_f G^\circ_m$ (kJ mol^{-1})	$\Delta_f H^\circ_m$ (298.15 K) (kJ mol^{-1})	S°_m (298.15 K) (J K^{-1} mol^{-1})
$BaNd_2Fe_2O_7$(s)	$-3400.5 + 0.6987(T\,(K))$ $(840 \le T\,(K) \le 989)$	−2756.9	234.0
$BaNdFeO_4$(s)	$-2034.7 + 0.4398(T\,(K))$ $(861 \le T\,(K) \le 995)$	−2061.5	91.6

3.4. Gibbs energy of formation for $BaNdFeO_4$(s)

The variation of reversible e.m.f. values of cell (III) as a function of temperature is shown in Fig. 6. The e.m.f. data were least squares fitted to yield the following linear relation:

$$E_{III}\,(V)\,(\pm 0.002) = -0.3068 + 3.8122\times10^{-4}(T\,(K)) \quad (861 \le T\,(K) \le 995). \tag{19}$$

The half-cell reactions associated with cell (III) can be written as:

$$CaF_2(s) + \tfrac{1}{2}O_2(g) + 2e^- \rightarrow CaO(s) + 2F^- \quad (\text{at } +\text{ve electrode}), \tag{20}$$

and

$$2BaNdFeO_4(s) + 2F^- \rightarrow BaNd_2Fe_2O_7(s) + BaF_2(s) + \tfrac{1}{2}O_2(g) + 2e^- \quad (\text{at } -\text{ve electrode}). \tag{21}$$

The net virtual cell reaction associated with cell (III) can be written as:

$$2BaNdFeO_4(s) + CaF_2(s) \rightarrow CaO(s) + BaNd_2Fe_2O_7(s) + BaF_2(s). \tag{22}$$

The Gibbs energy change, $\Delta_r G^\circ(T)$, for reaction (22) can be calculated by using Eqs. (11) and (19) and can be given by:

$$\Delta_{r(22)}G^\circ(T)\,(\text{kJ mol}^{-1})\,(\pm 0.4) = -59.2 + 0.0736(T\,(K)) \quad (861 \le T\,(K) \le 995). \tag{23}$$

The values of $\Delta_f G^\circ_m$ ($BaNdFeO_4$, s) were obtained by using Eq. (23) and values of $\Delta_f G^\circ_m(T)$ for $BaNd_2Fe_2O_7$(s) from Eq. (18) and $\Delta_f G^\circ_m(T)$ for CaO(s), CaF_2(s) and BaF_2(s) from Table 1 and can be given by:

$$\Delta_f G^\circ_m\,(BaNdFeO_4, s)\,(\text{kJ mol}^{-1})\,(\pm 1.5) = -2034.7 + 0.4398(T\,(K)) \quad (861 \le T\,(K) \le 995). \tag{24}$$

3.5. Second law analysis

The second law analysis of thermodynamic data is explained in detail in literature [7]. In this method, one can calculate the values of $\Delta_f H^\circ_m$ (298.15 K) and S°_m (298.15 K), if the thermal functions or heat capacities of the reactants and products and the phase transition or any magnetic order–disorder transitions are known. The two compounds $BaNd_2Fe_2O_7$(s) and $BaNdFeO_4$(s) do not show any phase transition or magnetic order–disorder transitions during heat capacity measurement in the measured temperature range. Based on the heat capacities and standard molar Gibbs energies of formation obtained in this study and the values of molar heat capacities of Ba(s), Fe(s), O_2(g) and Nd(s) from literature [4], the values of $\Delta_f H^\circ_m$ (298.15 K) and S°_m (298.15 K) for the two compounds $BaNd_2Fe_2O_7$(s) and

Table 3
Thermodynamic functions for the compound $BaNd_2Fe_2O_7$(s)

T (K)	$C^{\circ a}_p$ (J K^{-1} mol^{-1})	H° (J mol^{-1})	G° (J mol^{-1})	S° (J K^{-1} mol^{-1})	$H^\circ_T - H^\circ_{298.15}$ (J mol^{-1})	$\Delta_f H^\circ$ (J mol^{-1})	$\Delta_f G^\circ$ (J mol^{-1})	fef
298.15	266.6	−2756900.0	−2826667.1	234.0	0	−2756900.1	−2535422.9	234.0
300	267.1	−2756406.3	−2827101.5	235.6	493.7	−2756842.1	−2534048.8	234.0
350	278.2	−2742766.1	−2839954.7	277.7	14133.9	−2755129.3	−2497048.6	237.3
400	288.1	−2728603.5	−2854799.5	315.5	28296.5	−2753269.9	−2460306.1	244.8
450	297.2	−2713966.9	−2871448.1	349.9	42933.1	−2751404.5	−2423798.1	254.5
500	305.9	−269885.1	−2889750.5	381.7	58014.9	−2749627.8	−2387493.9	265.7
550	314.3	−2683376.8	−2909584.3	411.3	73523.2	−2748011.7	−2351360.3	277.6
600	322.5	−2667454.2	−2930848.3	438.0	89445.8	−2746224.4	−2315370.3	288.9
650	330.6	−2651125.9	−2953457.2	465.1	105774.1	−2743876.3	−2279562.0	302.4
700	338.5	−2634397.9	−2977338.4	489.9	122502.1	−2741677.5	−2243929.0	314.9
750	346.4	−2617274.7	−3002429.3	513.5	139625.3	−2739654.8	−2208447.3	327.3
800	354.2	−2599759.7	−3028675.4	536.1	157140.3	−2737507.8	−2173100.4	339.7
850	361.7	−2581855.5	−3056028.8	557.8	175044.5	−2735244.9	−2137894.5	351.9
900	369.7	−2563563.9	−3084447.2	578.7	193336.1	−2733066.2	−2102819.7	363.9
950	377.4	−2544886.6	−3113892.8	598.9	212013.4	−2731042.7	−2067862.1	375.7
1000	385.1	−2525824.9	−3144331.9	618.5	231075.1	−2729279.5	−2033004.9	387.4

[a] Smoothed values of $C^\circ_{p,m}$.

Table 4
Thermodynamic functions for the compound $BaNdFeO_4$(s)

T (K)	C_p°[a] (J K^{-1} mol^{-1})	H° (J mol^{-1})	G° (J mol^{-1})	S° (J K^{-1} mol^{-1})	$H_T^{\circ} - H_{298.15}^{\circ}$ (J mol^{-1})	$\Delta_f H^{\circ}$ (J mol^{-1})	$\Delta_f G^{\circ}$ (J mol^{-1})	fef
298.15	153.6	−2061500.0	−2088810.5	91.6	0	−2061500.1	−1918592.0	91.6
300	153.9	−2061215.5	−2088980.9	92.6	284.4	−2061473.1	−1917705.4	91.7
350	161.9	−2053317.8	−2094227.3	116.9	8182.2	−2060627.1	−1893808.2	93.5
400	169.4	−2045032.7	−2100632.5	139.0	16467.3	−2059653.5	−1870042.6	97.8
450	176.7	−2036377.5	−2108098.4	159.4	25122.5	−2058653.7	−1846401.4	103.6
500	183.8	−2027362.5	−2116547.3	178.4	34137.5	−2057696.6	−1822869.7	110.1
550	190.8	−2017994.3	−2125916.4	196.2	43505.7	−2056835.4	−1799429.7	117.1
600	197.8	−2008277.1	−2136153.7	213.1	53222.9	−2055722.6	−1776068.0	124.4
650	204.7	−1998214.1	−2147215.8	229.2	63285.9	−2053954.7	−1752835.4	131.8
700	211.6	−1987807.4	−2159065.7	244.6	73692.6	−2052228.6	−1729737.5	139.3
750	218.4	−1977058.6	−2171671.5	259.5	84441.4	−2050556.3	−1706761.1	146.9
800	225.2	−1965968.8	−2185005.5	273.8	95531.2	−2048621.7	−1683900.6	154.4
850	232.0	−1954539.1	−2199043.4	287.6	106960.9	−2046413.1	−1661172.6	161.8
900	238.8	−1942770.0	−2213763.9	301.1	118730.0	−2044104.9	−1638577.6	169.2
950	245.5	−1930662.1	−2245178.1	314.2	130837.9	−2041731.9	−1616112.8	176.5
1000	252.3	−1918216.0	−3144331.9	326.9	143284.0	−2039346.0	−1593773.6	183.6

[a] Smoothed values of $C_{p,m}^{\circ}$.

$BaNdFeO_4$(s) have been calculated assuming no oxygen non-stoichiometry and summarized in Table 2. Thermodynamic functions like $S^{\circ}(T)$, $C_p^{\circ}(T)$, $H^{\circ}(T)$, $\{H^{\circ}(T) - H^{\circ}(298.15\,K)\}$, $G^{\circ}(T)$, free energy function (fef), $\Delta_f H^{\circ}(T)$ and $\Delta_f G(T)$ are calculated from 298 to 1000 K for $BaNd_2Fe_2O_7$(s) and $BaNdFeO_4$(s) and represented in Tables 3 and 4, respectively. The values of thermochemical data generated in this study will enable the assessment of thermochemical stabilities of these two oxides in different chemical environments.

Acknowledgments

The authors are thankful to Dr. K.D. Singh Mudher and Dr. K. Kirshnan for X-ray diffraction analysis.

References

[1] M. Vallino, F. Abbattista, D. Mazza, Mater. Res. Bull. 21 (1986) 733–738.
[2] C.M. Jantzen, F.P. Glasser, Mater. Res. Bull. 14 (1979) 1601–1607.
[3] G.W.H. Hohne, W.F. Hemminger, H.-J. Flammershein, Differential Scanning Calorimetry, second ed., Springer-Verlag, Berlin, Heidelberg, New York, 2003.
[4] M.W. Chase Jr., JANAF Thermochemical Tables, fourth ed., J. Phys. Chem. Ref. Data, Monograph No. 9, 1995.
[5] S.K. Rakshit, S.C. Parida, Z. Singh, R. Prasad, V. Venugopal, J. Solid State Chem. 177 (2004) 1146–1156.
[6] S.C. Parida, S. Dash, Z. Singh, R. Prasad, K.T. Jacob, V. Venugopal, J. Solid State Chem. 164 (2002) 34–41.
[7] E.D. Cater, in: R.A. Rapp (Ed.), Physicochemical Measurements in Metals Research, Part I, in: R.F. Bunshah (Ed.), Techniques of Metals Research, vol. IV, Interscience Publishers, 1970.